From the Department of Clinical Neuroscience and
Center for Hearing and Communication Research,
Karolinska Institutet, Stockholm, Sweden

COCHLEAR MECHANICS UNLEASHED; DESIGN AND APPLICATION OF SUPERRESOLUTION TECHNIQUES IN THE COCHLEAR APEX

Stefan Jacob

Karolinska Institutet

Stockholm 2011

All previously published papers were reproduced with permission from the publisher.
Published by Karolinska Institutet. Printed by US-AB, Solna, Sweden.

ISBN 978-91-7457-323-7

to an amazing and wonderful woman

Hearing is one of the five traditional senses. Next to vision it is probably the most important for man and plays a crucial role in day-to-day communication. However, hearing is extremely challenged by modern life style, due to increasing noise exposure and aging societies. Ten percent of the world population is estimated to be hearing impaired. Unfortunately, most conditions cannot be treated sufficiently, a fact often attributed to the very limited understanding of inner ear workings. Early on, it was recognized that the sensitivity of the ear is dramatically enhanced by an active process, termed cochlear amplification, which remains enigmatic.

The first part of this thesis presents two complementary optical techniques to measure vibration amplitudes, which are orders of magnitude smaller than the wavelength of light. Both methods are adapted to probe the physiologically relevant low frequency part of the organ of Corti, which is responsible for speech reception. In the second part of the thesis we employ these methods to investigate the role of the large electrochemical potential surrounding the hearing organ. This endogenous extracellular potential is hypothesized to play an important role in cochlear amplification, but its immediate impact on cochlear mechanics is highly speculative. We show that the endocochlear potential leads to sustained deformations of the hearing organ and spatially distinctive alterations of the mechanical response to sound perception.

The third part of the thesis investigates the role of membrane cholesterol in somatic hair cell motility, which is one of two mechanisms hypothesized to underlie cochlear amplification. We show that reducing cholesterol dramatically affects the interaction of the hearing organ with the endocochlear potential.

LIST OF PUBLICATIONS

The thesis is based on the following papers.

- Jacob S., I. Tomo, A. Fridberger, J. Boutet de Monvel, and M. Ulfendahl. 2007. Rapid confocal imaging for measuring sound-induced motion of the hearing organ in the apical region. Journal of Biomedical Optics. 12:021005.
- Jacob S., C. Johansson, M. Ulfendahl, and A. Fridberger. 2009. A digital heterodyne laser interferometer for studying cochlear mechanics. Journal of Neuroscience Methods. 179:271-7.
- Jacob S., M. Pienkowski, and A. Fridberger. 2011. The endocochlear potential alters cochlear micromechanics. *Accepted in* Biophysical Journal
- Brownell W.E., S. Jacob, P. Hakizimana, M. Ulfendahl, and A. Fridberger. 2011. Membrane cholesterol modulates cochlear electromechanics. *In press* Pflügers Archiv : European Journal of Physiology.

CONTENTS

1 INTRODUCTION 1

1.1 THE EAR . . . 1

1.2 THE MIDDLE EAR . . . 1

1.3 THE INNER EAR . . . 2

1.3.1 THE COCHLEA . . . 2

1.3.2 COCHLEAR HAIR CELLS . . . 4

1.3.3 THE ORGAN OF CORTI . . . 10

1.4 CHOLESTEROL . . . 13

1.5 THE AIM OF THE THESIS . . . 14

2 MATERIALS & METHODS 15

2.1 TEMPORAL BONE PREPARATION . . . 15

2.2 CONFOCAL MICROSCOPY . . . 16

2.2.1 TIME-RESOLVED CONFOCAL MICROSCOPY . . . 18

2.3 INTERFEROMETRY . . . 20

2.3.1 HOMODYNE INTERFEROMETRY . . . 20

2.3.2 HETERODYNE INTERFEROMETRY . . . 21

3 RESULTS 23

3.1 RESULTS OF PAPER I . . . 23

3.2 RESULTS OF PAPER II . . . 24

3.3 RESULTS OF PAPER III . . . 25

3.4 RESULTS OF PAPER IV . . . 26

4 DISCUSSION 27

A HOMODYNE INTERFEROMETRY 39

B HETERODYNE INTERFEROMETRY 40

LIST OF FIGURES

1.1 SCHEMATIC VIEW OF THE EAR 1
1.2 SCHEMATIC CROSS-SECTION OF THE COCHLEA 3
1.3 SCHEMATIC VIEW OF STEREOCILIA 5
1.4 COCHLEAR HAIR CELL SCHEMATIC 6
1.5 EXCITATORY BUNDLE DEFLECTION 7
1.6 INHIBITORY BUNDLE DEFLECTION 7
1.7 HAIR CELL RECEPTOR POTENTIAL 8
1.8 SCHEMATIC CROSS-SECTION OF THE ORGAN OF CORTI 10
1.9 SCHEMATIC ORGAN OF CORTI VIBRATION PATTERN 11
2.1 PERFUSION OF THE TEMPORAL BONE 16
2.2 LASER SCANNING MICROSCOPE 17
2.3 HOMODYNE INTERFEROMETRY 21
2.4 HETERODYNE INTERFEROMETRY 22

ABBREVIATIONS

a.u.	**A**rbitrary **U**nits
BM	**B**asilar **M**embrane
CL	**C**ortical **L**atice
EP	**E**ndocochlear **P**otential
HC	**H**ensen's **C**ell
IHC	**I**nner **H**air **C**ell
i.p.	**I**ntra**p**eritoneal
LSM	**L**aser **S**canning **M**icroscope
MEM	**M**inimum **E**ssential **M**edium
OHC	**O**uter **H**air **C**ell
RL	**R**eticular **L**amina
RM	**R**eissner's **M**embrane
SM	**S**cala **M**edia
SPL	**S**ound **P**ressure **L**evel
SSC	**S**ub**s**urface **C**isternae
ST	**S**cala **T**ympani
SV	**S**cala **V**estibuli

1 INTRODUCTION

1.1 THE EAR

The typical mammalian ear is subdivided into three parts: the outer, the middle and the inner ear, Figure 1.1. The outer ear is the visible part, which includes the pinna, the auditory canal and the tympanic membrane (ear drum). The primary function of the outer ear is to guide the sound to the tympanic membrane. At the tympanic membrane sound leads to an oscillatory pressure difference between the air in the auditory canal and the air in the middle ear cavity. These pressure differences force the tympanic membrane to vibrate. Due to its shape, the pinna and auditory canal can act like a resonant cavity, which makes the outer ear transfer function complex.

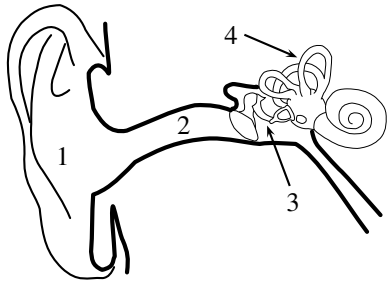

Figure 1.1: *Schematic illustration of the ear. The outer ear includes the pinna (1) and ear canal (2) and is separated by the tympanic membrane from the middle ear (3), which includes the three ossicles. The inner ear (4) includes the snail-like hearing organ and the semicircular canals of the balance organ.*

1.2 THE MIDDLE EAR

The air filled middle ear cavity accommodates the three ossicles: malleus (hammer), incus (anvil) and stapes (stirrup). The malleus is attached to the tympanic membrane, while the stapes is attached to the oval window, a membrane separating the middle ear from the fluid filled inner ear. The malleus and stapes are connected *via* the incus. This means that the tympanic membrane is coupled to the oval window and that the sound-evoked vibrations of the tympanic membrane are conducted to the inner ear. Since the inner ear is fluid filled, the middle ear transfers pressure oscillations from air into fluid, a process, which is hampered by the different densities of air

and water. In the ear the density mismatch is partially compensated by an air interface (tympanic membrane), which is approximately 20 times larger than the water interface (oval window). Furthermore, the leverage function of the ossicles contributes to the high transmission yield achieved in the middle ear. In order to adapt the air pressure in the middle ear cavity to the slowly varying air pressure of the environment, the middle ear is connected to the throat *via* the Eustachian tube. The tube opens only briefly while yawning or swallowing and stays closed otherwise to avoid disturbing the middle ear.

1.3 THE INNER EAR

The sensory organs for hearing and balance are located in the bone-enclosed inner ear. The vestibular apparatus, which is the organ of balance, consists of three canals, the saccule and utricle. In general the three canals: the horizontal (lateral), the anterior semicircular (superior) and the posterior (inferior) semicircular canal are almost orthogonal to each other and are used to detect rotational head movements. The underlying operating principle is similar to a cup filled with liquid; the cup can be rotated but the liquid will not rotate. Each semicircular canal contains a soft structure (cupula), which is attached to the canal and acts as an impediment for the fluid flow. Canal rotation forces the cupula to move through the fluid, deflecting the cupula from its resting position. Specialized hair cells detect this deflection and transmit the signal to the brain stem *via* the vestibulcochlear nerve (CN VIII). A similar setup is used by the saccule and utricle to detect vertical head movements and head tilting, respectively.

1.3.1 THE COCHLEA

The sensory organ for hearing is located in a second distinct part of the inner ear: the cochlea, Figure 1.2. The cochlea is built up like a coiled shell and the number of turns is species dependent and ranges typically between two and four. It consists of three fluid filled compartments: the scala vestibuli (SV), the scala tympani (ST) and the scala media (SM). These compartments are arranged in a sandwich like manner with ST at the bottom, SV at the top and SM in the

middle of the tube. At the apical end of the cochlea, in a place called helicotrema, merges SV and ST. The SV and ST are filled with perilymph, a fluid of comparable ionic composition to typical extracellular fluid (rich in sodium) [62]. On the other hand, SM is filled with endolymph, which is comparable to intracellular fluid (rich in potassium) [62]. Stria vascularis, a dedicated multicellular structure at the radial border of SM, continuously replenishes the potassium and keeps SM at a large positive electro-chemical potential with respect to the perilymph filled SV and ST (endocochlear potential) [50, 31]. In order to prevent leakage, SM is separated from SV by Reissner's membrane (RM), which consists of a base membrane and a tight inner and outer cell layer [29]. On the other side, SM is divided from ST by the basilar membrane (BM), on which the actual hearing organ, the organ of Corti, rests.

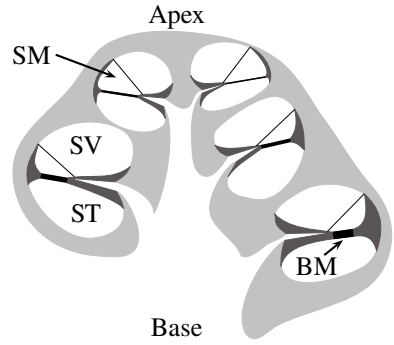

Figure 1.2: *Schematic cross-section of the cochlea and illustration of its three fluid filled compartments: scala vestibuli (SV), scala tympani (ST) and scala media (SM). Note that the basilar membrane (BM) gets wider and softer towards the cochlear apex.*

The bony enclosure of the inner ear has two distinct openings, composed only of a flexible membrane to protect the inner ear fluids from the air in the middle ear cavity. Both openings, called windows, are located at the basal part of the cochlea. The so-called round window is positioned at ST, while the previously mentioned oval window, which is covered by the stapes, is located at SV. During acoustic stimulation of the ear, the vibrating stapes pushes and pulles on the oval window, generating oscillating pressure differences between SV and ST. These pressure differences propagate along the cochlear spiral and force the flexible structures between ST and

SV, namely RM and the complex formed by the BM and the organ of Corti, to vibrate. The fact that the BM is narrow and stiff at the basal part of the cochlea and gradually gets wider and softer towards the apical part makes the propagating pressure difference accumulate dispersion [13]. This decreases wave length and group velocity in a frequency dependent manner. The further the group velocity declines the more increases the amplitude of the BM – organ of Corti vibrations, which in turn decline rapidly as the group velocity approaches zero due to dissipation of the energy. Because of the frequency dependence of the dispersion process, each frequency leads to maximal BM vibration amplitudes at a different location along the cochlear spiral. High frequencies have a maximal vibration amplitude in the cochlear base and low frequencies in the apex [5]. The frequency, to which a given cochlear location responses most, is called characteristic or best frequency of this location. Subsequently, the organ of Corti converts the BM vibrations into bioelectrical information, which are conveyed to the brainstem by the vestibulcochlear nerve.

1.3.2 COCHLEAR HAIR CELLS

The key component of the organ of Corti are the elongated sensory hair cells, which can detect the deflection of their "hairs" [20]. At the apical cell end the cochlear sensory cells have a hair bundle made of stereocilia, which are rod-like cell membrane protrusions around an actin core, Figure 1.3 [21]. The densely packed parallel actin filaments in the stereocilia are crosslinked by esprins, fimbrins and plastins and form an almost crystalline structure [65, 73, 15]. Furthermore, stereociliar actin turnover is approximately one order of magnitude slower than in comparable structures, suggesting a heavy regulation of actin dynamics [58]. The actin core dominates the mechanical properties of the stereocilia, e.g. bending modulus, and is therefore of highest importance for hair cell function, as bundle bending can be detrimental for deflection [72]. Some of the stereocila actin filaments extent into the hair cell soma and form so-called rootlets (review [66]). These rootlets connect to a rigid and dense actin network in the apical part of the hair cell cytoplasm, the cuticular plate. Addition-

ally, the cuticular plate is anchored to the cytoskeleton *via* microtubules [37]. It is thought to contribute to stereocilia function by forming a rigid reference structure. Stereocilia are tapered around their attachment point at the hair cell soma, forming a neck-like structure that eases hair bundle deflection. Hair cell sensitivity is further increased by lateral links, which crosslink neighboring stereocilia in one hair bundle and damp thereby thermal vibrations [54]. Typically, a hair bundle consists of different rows of stereocilia, Figure 1.4. Every row has a characteristic stereocilia length, which is maintained throughout the life of the mature hair cells (review [66]). The rows are parallel to each other and ordered according to the stereocilia height, which gradually increases from one side of the cuticular plate to the opposite site.

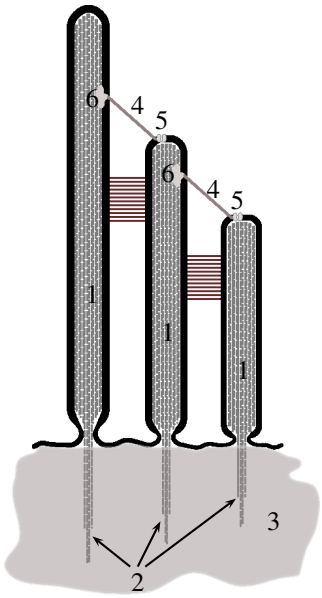

Figure 1.3: *Schematic cross-section of the stereocilia rows. The dense actin core (1) of the sterocilium extends as rootlets (2) into the cuticular plate (3). Tip links (4) probably connect the mechanotransduction channel (5) with an adaptation motor (6) in the neighboring stereocilium.*

A deflection of the hair bundle parallel to the rows fails to elicit any kind of observable response from the hair cells [20]. On the other hand, deflection of the hair bundle towards the tallest row of stereocilia poses an excitatory input, while deflection towards the smallest row is inhibitory [20, 16]. Thus, hair cells are not just polarized by the clear distinction between cell apex and base, but also by the excitatory / inhibitory deflection direction of the hair bundle. In

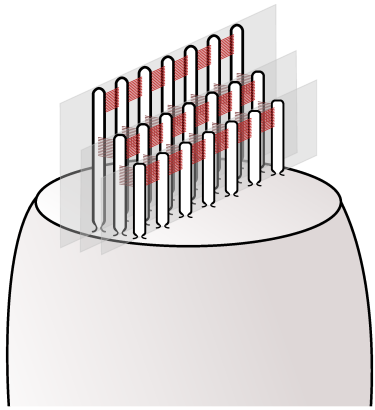

Figure 1.4: *Schematic view of a cochlear hair cell. The apical part of the hair cell is flattened and decorated with rows of stereocilia, which are interconnected.*

electron micrographs it has been shown that a fine physical connection exists between neighboring stereocilia tips of different rows, coupling the taller stereocilia with the smaller one, Figure 1.3 [54]. These connections are called tip links and are build up of two distinct transmembrane membrane proteins. The upper part of the link is made of a Cadherin (CDH23) dimer, while the lower part is made of Protocadherin (PCDH15) dimer [39]. The link is formed due to interaction of the N termini of the two dimers. In the smaller stereocilia, the tip link connects to a mechanotransduction channel of unknown molecular composition. This channel is cation selective with a high permeability for Ca^{2+} and K^{+} (review [9]). It is similar in its physiology and pharmacological profile to other mechanotransduction channels found in mechanosensory neurons (review [17]). On the other end, the tip link is thought to be connected to myosin motors, which allow a slow regulation of the tension between tip link and mechanotransduction channel (review [27]). This regulation ensures that approximately 10 % of the mechanotransduction channels are open at rest. Upon excitatory deflection of the hair bundle, “tip link tension“ increases, which increases the open probability of the mechanotransduction channel. On the other hand, inhibitory deflection decreases the open probability, Figure 1.5 and Figure 1.6.

Cochlear sensory cells have a negative equilibrium membrane potential, which forms together with the posi-

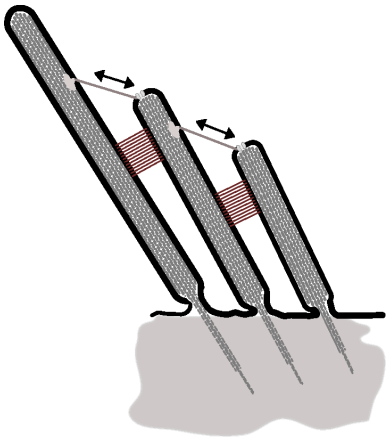

Figure 1.5: *Cross-section of greatly exaggerated excitatory bundle deflection. Note that the force, leading to bundle deflection, acts only on the tip of the largest stereocilium. Bundle deflection initially raises tip link tension, which increases the open probability of the MET channel. Prolonged deflection leads to a fast calcium-mediated adaptation of the MET channel, followed by a release of the tip link tension mediated by the adaptation motor.*

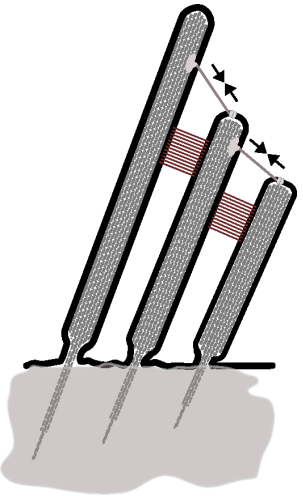

Figure 1.6: *Cross-section of greatly exaggerated inhibitory bundle deflection. Bundle deflection initially lowers tip link tension, thereby decreasing the open probability of the MET channel. Prolonged bundle deflection leads to adaptation.*

tive EP a large electro-chemical gradient across the mechanotransduction channels. Thus, even at rest, hair cells are statically depolarized by the small cation influx through the open mechanotransduction channels [60]. During inhibitory bundle deflection, this influx decreases in relation to the size of the bundle deflection, hyperpolarizing the hair cell [30]. On the other hand, during excitatory bundle deflection, the ion influx increases, further depolarizing the cell. The relation between the ampli-

tude of the bundle deflection and cell polarization changes is highly nonlinear, Figure 1.7 [13]. While inhibitory bundle deflections have only a modest effect on cell polarization, excitatory deflections lead to large changes. As cochlear hair cells are evolved to detect sound, a rapidly alternating signal, hair cells have the ability to adapt to prolonged unidirectional bundle deflection [18]. A sustained excitatory bundle deflection increases calcium concentration in the bundle, which in turn disables the mechanotransduction channel on a timescale of a few hundred μs [56]. The remaining "tip link tension" is thought to be relieved *via* the myosin on the upper tip link ($\tau \sim$ 100 ms). The calcium dependent closure of the mechanotransduction channels is hypothesized to be the basis of active hair bundle movements. It has been shown, mainly in non-mammals, that hair bundles can generate mechanical forces and that they can spontaneously oscillate [10]. Such a mechanism has the potential to decrease hearing thresholds and increase frequency selectivity by actively amplifying its hair bundle deflection.

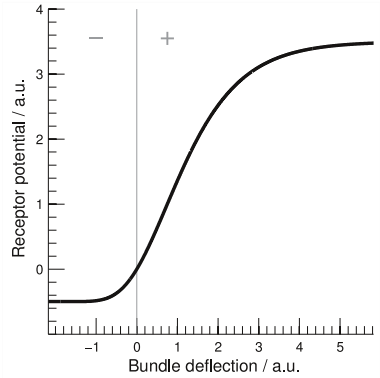

Figure 1.7: *Greatly simplified hair cell receptor potential. Graph illustrates the asymmetry of the cell polarization changes evoked by inhibitory (-) and excitatory (+) bundle deflections.*

The mammalian hair cells have evolved into two distinct subpopulations: inner hair cells and outer hair cells. Inner hair cells perform the classical hair cell duty: converting mechanical stimuli into bioelectrical signals. Therefore, inner hair cells have a strong and highly precise synaptic transmission due to ribbon synapses at

the presynaptic site [63, 42]. Another distinct feature is the wide inner hair cell bundle, which formes a single line, spanning almost the entire cuticular plate.

The cylindrical outer hair cells, which have been the focus of cochlear mechanics research for the last 25 years, have the ability to decrease hearing thresholds and increase frequency discrimination due to their active mechanical feedback on organ of Corti vibrations (review [3]). It has been shown that isolated outer hair cells respond to cell hyperpolarization with active cell elongation, while they shorten during depolarization [6, 2]. This somatic electromotility is very fast and isolated outer hair cells are able to elongate and contract even at very high frequencies (>70 kHz) [22]. Somatic electromotility has been attributed to a unique outer hair cell protein, prestin, which is a member of the solute carrier family 26 [71]. This family of membrane transport proteins is generally refered to as multifunctional anion exchangers. Mammalian prestin is found as oligomeres in the plasma membrane of outer hair cells and appears to be mutated in such a way that it can not complete the exchange cycle [3, 67]. Instead, prestin, which, increases electromotility and non-linear capacity of the cell soma. The importance of prestin becomes apparent in prestin knock-out mice, which show large elevated hearing thresholds [44, 14]. Additionally, morphology makes outer hair cells stand apart from other hair cells. The hair bundle of outer hair cells is, instead of being a straight line, formed like a W or V and the OHC nucleus is located at the very basal end of the cell soma. Intracellular, in close proximity to the lateral plasma membrane, is a network of stacked membranous sheets, called the subsurface cisternae (SSC). The surface of the SSC, which faces the plasma membrane, is lined with a patchwork of domains of parallel actin fibers, the cortical lattice (CL) [32]. These domains seem to be connected to the plasma membrane *via* pillar-like structures of unknown molecular origin [25]. The function of the SSC-CL-Pillar complex is highly disputed, but the complex is believed to be involved in membrane recycling and maintaining the cylindrical shape of the

outer hair cells.

1.3.3 THE ORGAN OF CORTI

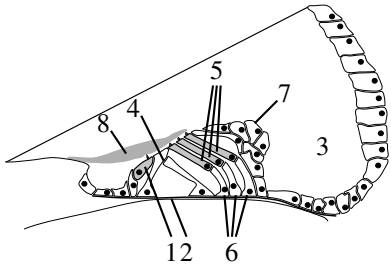

Figure 1.8: *Schematic cross-section of the apical organ of Corti. IHC (1), BM (2), SM (3), pillar cells (4), OHCs (5), Deiters' cells (6), Hensen's cells (7), TM (8)*

The location of the hair cells in the organ of Corti is highly regulated. They are arranged in rows along the organ of Corti spiral, from apex to base. Typically, a single row of inner hair cells (IHC) is followed by three, seldom four or five, parallel rows of outer hair cells (OHC), which are located more radially than the IHCs, Figure 1.8. The number of hair cells is highly species dependent: 4.500 in rats, 12.500 in cats and 17.000 in Dolphins and man [47, 68]. The inner hair cell soma is located right on top of the bony ridge, anchoring the BM, while the hair bundle is free-standing in scala media. Between the inner and outer hair cells is a group of supporting cells, the pillar cells. These cells rest on the basilar membrane and form two perilymph filled compartments inside the organ of Corti (tunnel of Corti / space of Nuel). The heads of the pillar cells form a tight connection between the IHC apex and the apex of the first row of OHCs. The integration of the OHCs into the organ of Corti is highly specialized and accounts for their somatic electromotility. Each OHC sits on a supporting cell, called Deiters' cell, which forms a cup around the very basal end of the OHC. Additionally, the Deiters' cells form thin phalangeal processes, which connect to the reticular lamina (RL), a membrane covering the entire scala media-facing surface of the organ of Corti, only sparing the hair cells. The main part of the OHC soma is surrounded by perilymph in the space of Nuel, which connects to the outer tunnel. The radial wall of the outer tunnel is formed by the Hensen's cells, supporting cells which build up the

radial part of the organ of Corti.

On top of the organ is the tectorial membrane (TM), a highly ordered collagen-rich extracellular matrix, which is anchored to the organ more medially than the IHCs (review [64]). The TM floats parallel to the RL and makes contact only with the tallest row of OHC stereocilia, but not with the IHC bundle. Even though the basic anatomy of the organ of Corti is similar between its high frequency and its low frequency end, there are still significant differences, which represent the adaptation to the spatial frequency separation. One of the most eye-striking adaptations is the OHC length, with increasing distance to the oval window increases gradually the size of the OHC soma and the length of the sterocila. OHCs, which encode for high frequencies, are short, firmly anchored in the Deiters' cell cup, perpendicular oriented to the BM and their longest stereocilia are firmly embedded in a massive TM. On the other hand, OHC, encoding for low frequencies, are long, loosely anchored in the Deiters' cell cup and rotated towards the BM, so that OHCs and BM form an angle of approximately 60 degrees. Furthermore, the TM at the low frequency end is thinner and not as firmly attached to the OHC bundle. The gradually changing angle between OHCs and BM coincides with a change of RL orientation. At the cochlear base, the RL is parallel to the BM, while they form an angle of approximately 30 degrees in the very apex.

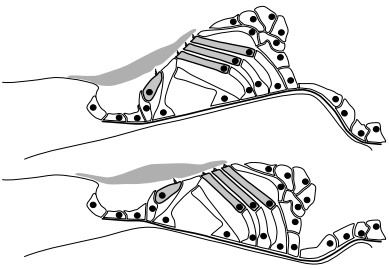

Figure 1.9: *Cross-sections of greatly exaggerated organ of Corti vibration patterns. The upper schematic shows the organ of Corti following the BM upward motion. Shearing forces between the RL and TM deflect the OHC bundles in the excitatory direction. The lower schematic shows the downward motion and the OHC bundles are deflected in the inhibitory direction.*

It is generally accepted that the response of the organ of Corti to loud (not

harmful) sounds is dominated by the passive mechanical properties of the hearing organ (review: [57]). The acoustic energy of the loud sound makes the BM vibrate, which in turn makes the organ of Corti vibrate, Figure 1.9. In this intensity range, it is believed that the RL vibration pattern follows the sound-evoked vibration of the BM. This leads to shearing between the RL and TM, which in turn results in alternating deflection of the OHC bundle. The IHC bundle oscillations have a different phase than the OHC bundles, reflecting the free-standing nature of the IHC bundle. Unfortunately, this model fails to explain the amazing frequency discrimination observed in psycho-acoustical measurements. Furthermore, the hearing threshold of the described model is much higher than the actual threshold observed in living mammals. In order to bridge the gap to the *in vivo* observations the model was extended by a hypothetical process: the cochlear amplifier, termed already in 1948 [28].

Cochlear amplification is widely studied on high frequency BM motion in the *in vivo* cochlear base, which shows a dramatic change of vibration patterns with decreasing stimulus intensity (review: [57]). First, the characteristic frequency, which elicits a maximum vibration response, gradually shifts to higher frequencies with decreasing sound intensities. Furthermore, the frequency response becomes more sharply tuned and the sensitivity of the BM to sound pressure greatly increases with decreasing sound intensities. The literature has credited most of this to somatic electromotility, since prestin inhibited or prestin knock-out animals do not show the benefits of cochlear amplification [44, 14]. In the cochlear base the actively modified BM vibration was shown to correspond to the tuning of auditory nerve fibers [48] (but see also [19]). Anyhow, various models and theories try to explain cochlear amplification and compete for acceptance. Therefore the following paragraph is a very subjective compilation of some of them.

It has been shown that coupling similar motile hair bundles together might lead to a sharpened frequency response, accompanied by an increased intensity-dependent sensitivity [4]. The reader

shall be reminded that such a coupling is found in the organ of Corti among the OHC bundles, which are elastically connected through the TM. Similar to the observed BM data, hair bundle sensitivity would increase with decreasing stimulus level. Consequently, weak BM vibrations lead to actively enhanced deflections of the OHC bundle, increasing OHC mechanotransduction and enhancing the electromotile response of the OHC soma. A part of this response would feed back to the BM and lead to the observed BM vibration pattern, depending on the temporal and spatial relation between feedback and BM vibration. However, the impact of the active mechanisms on the RL vibration is highly speculative. The assumption that the feedback at the level of the BM and the RL is of similar polarity is not warranted, and more direct evidence is needed to understand RL motion patterns [41, 45].

1.4 CHOLESTEROL

The steroid cholesterol is an essential part of eukaryotic cell membranes [1]. It modifies the ion permeability of the membrane and alters membrane fluidity. Furthermore, cholesterol is believed to be a vital part of lipid rafts, which play an important role in compartmentalization of the plasma membrane (review [43]). Again, OHCs stand apart from ”normal” cells. They do show an anisotropic distribution of membrane cholesterol, with a high content in the apical and basal cell end and a low cholesterol concentration in the lateral wall, indicating a tight regulation of the cholesterol concentration [49, 70]. The cholesterol distribution in the plasma membrane of OHCs is inverse to the distribution of prestin, suggesting detrimental cholesterol-prestin interactions. It has been shown that cholesterol affects the electrical fingerprint of somatic electromotility, presumably by interfering with prestin. In isolated OHCS, an increase in cholesterol leads to a decrease and hyperpolarizing shift of the prestin-associated charge movement, indicating a reduced somatic electromotility [55, 61]. Thus, the inverse distribution of cholesterol and prestin seems necessary, as cholesterol negatively affects prestin. However, the effect on somatic

electromotility needs to be established.

1.5 THE AIM OF THE THESIS

As indicated in the previous chapters, many questions regarding the cochlear function are still unanswered. The primary goal of this thesis is to investigate cochlear mechanics in the low-frequency part of the hearing organ, which is important for speech encoding. We strive to understand how the active mechanisms affect the sound-evoked RL vibration patterns. This includes the question, if the OHC-mediated feedback is spatially invariant along the radial direction of the organ of Corti, which is often assumed unsaid. In order to answer these questions, a measurement platform is necessary, which allows us to easily alter the feedback amplitude. Such a platform would be useful to validate and compare different manipulations affecting cochlear mechanics, like cholesterol reduction, and facilitate our understanding of cochlear mechanics.

2 MATERIALS & METHODS

2.1 TEMPORAL BONE PREPARATION

All preparations and experiments are carried out at room temperature ($\sim$ 21°C) and are approved by the swedish authorities. Young albino or pigmented guinea pigs of both sexes, weighing 250 – 400 g, are anesthetized with an i.p. injection of sodium pentobarbital and decapitated. The temporal bone is quickly but gently removed from the skull and is fastened into a custom made holder. The middle ear cavity is carefully opened and the entire temporal bone is immersed in oxygenated tissue culture medium. The holder prevents leakage of the culture medium into the external ear canal and thereby allows the acoustic stimulation of the tympanic membrane. Due to the immersion of the middle ear, the tympanic membrane attenuates the effective sound pressure level (SPL) of the acoustic stimulus by approximately 30 dB SPL [7]. Following the submersion of the ear, two openings are made in the otic capsule to allow perfusion of scala tympani, Figure 2.1. A silicone tubing connects an elevated perfusion reservoir of continuously oxygenated tissue culture medium to a small hole in scala tympani of the basal turn. The second opening is made in the apical turn scala vestibuli, which serves as a drain for the perfusion and allows access to the apical organ of Corti. The perfusion does not just keep the preparation vital for up to 5 hours, it also allows to rapidly wash in pharmaceuticals and other chemicals, e.g. fluorescent dyes.

In the literature, it has been stated that upon death the endocochlear potential (EP) rapidly vanishes in a few minutes, but we found EPs as large as +50 mV 30 min after decapitation [52]. This apparent contradiction can be readily resolved by considering that anoxia is the main reason for the negative EP observed in dead cochleas. Surprisingly, re-oxygenation of animals, suffering from anoxia, quickly restores the positive EP and a moderate positive EP could be found in animals during hypoxia [26, 52]. Therefore re-oxygenation of the cochlea through the perfusion

quickly restores a moderate positive EP.

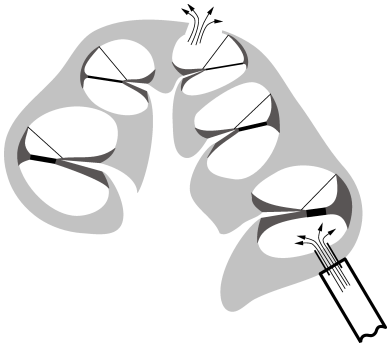

Figure 2.1: *Schematic of the temporal bone perfusion. The cross-section shows the opening in the cochlear base, which is connected to the perfusion tubing. The apical opening serves as perfusion outlet.*

In paper-**II**, **III** and **IV**, electrodes are advanced into scala media through the apical opening. They are freshly pulled and filled with electrolyte, which is either 3M KCL + 50 μM $CaCl_2$ or artificial endolymph (1.3 mM NaCl, 31 mM $KHCO_3$, 23 μM $CaCl_2$, 128.3 mM KCl; pH = 7.4; 300 mOsm). Both types are beveled to a low impedance ($\sim$2 M). The electrodes are used to repeatedly measure the amplitudes of the microphonic potential at various stimulus frequencies. This potential is a good indicator for the condition of the preparation. Furthermore, current injections into scala media are used to change scala media polarization. Positive current injection leads to a positive polarization of scala media in respect to the perilymph filled compartments, while negative current injection leads to negative polarization [33].

2.2 CONFOCAL MICROSCOPY

Laser scanning microscopy is the microscopy method of choice for high quality fluorescence images. Laser scanning microscopes (LSMs) have the unique ability to detect only fluorescence from the imaging plane. This is a huge advantage when imaging in "thick" samples. The basic principle is depicted in Figure 2.2. The classical LSM has at least one laser as excitation light source, followed by a dichroic beam splitter. This beam splitter reflects the excitation light, but has a high transmission for the stokes-shifted fluorescence. The excitation light is directed towards the microscope objective, which focuses the light into one single spot. The probability of

exciting a fluorescent molecule is highest in the focus spot and declines with increasing distance to the imaging plane in a quadratic manner. Nevertheless, fluorescence will be generated outside of the focus spot. The fluorescence, propagating towards the microscope objective, will be collected by the objective and guided to the dichroic mirror.

The fluorescence, transmitted through the dichroic mirror, is focused onto a pinhole, which will act as a barrier for fluorescence coming from outside of the excitation focus spot. The fluorescence, passing the pinhole, is detected by a point detector of choice, e.g. photomultiplier tube. Typically, a color filter is inserted into the light path before the pinhole to remove unwanted excitation light. It is apparent that the described setup does not immediately form an image, since it only illuminates a point. Therefore, similar to other scanning techniques, e.g. scanning electron microscopy, the sample needs to be imaged point by point by moving the excitation beam over the sample.

In a LSM, this is typically done by a scanning unit, consisting of two galvanic

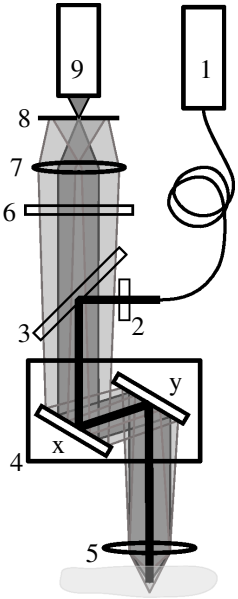

Figure 2.2: *Typical setup of an one-photon **L**aser **S**canning **M**icroscope and its operating principle. Components are excitation light source (1), excitation filter (2), dichroic beam splitter (3), scanning unit (4), microscope objective (5), emission filter (6), lens (7), pinhole (8) and a point detector (9). The excitation light path is depicted as the thick black line, while the florescence from the focal plane is illustrated in dark gray. Fluorescence originating from above or below the focal plane is depicted in light gray and blocked by the pinhole.*

mirrors, which scans the excitation beam over the sample. Even though the exposure time of a pixel is rather fast, (few μs), the acquisition time of an image is in the order of seconds, depending on the number of pixels to be acquired. This is much to slow to resolve the sound-evoked vibrations of the organ of Corti.

2.2.1 TIME-RESOLVED CONFOCAL MICROSCOPY

One peculiarity of scanning techniques is that the pixels in the final image are not just separated in space but also in time. The temporal separation is highly predictable and can be exploited to improve the temporal resolution of scanning techniques, provided the system under investigation shows temporal periodicity (period length > pixel dwell time).

Paper **I** describes a method called time-resolved confocal imaging [35]. With this method it is possible to generate images, in which all pixels are acquired at the same time, from ordinary confocal images. The first step is to match the periodicity to the image acquisition time, or vise versa.

$$(n * \frac{1}{N_i}) * T = t_{ac} \tag{1}$$

,where n denotes an arbitrary integer, N_i the number of images in the image series, T the period time of system under investigation and t_{ac} the image acquisition time. Therefore, the observed fl. intensity, $I[\mathbf{r}, t]$, acquired N_i times at a given spatial location **r** is equally spaced in the phase domain. It is straight forward to transform the time coordinate into a phase coordinate ($\phi_{n,\mathbf{r}}$) for every pixel.

$$\phi_{n,\mathbf{r}} = \frac{2\pi t_{n,\mathbf{r}}}{T} \tag{2}$$

, where $t_{n,\mathbf{r}}$ denotes the discrete time points of the pixel acquisition at the spatial location **r** in the n-th image. Hence the pixel intensity can be expressed as $I[\mathbf{r}, \phi_{n,\mathbf{r}}]$ and fourier rows can be used to reconstruct the intensity at any arbitrary phase ψ.

$$\begin{aligned} I[\mathbf{r}, \psi] &= \frac{1}{2} a_{0,\mathbf{r}} + \\ &+ \sum_{n=1}^{\alpha} a_{n,\mathbf{r}} cos[n\psi] + b_{n,\mathbf{r}} sin[n\psi] \end{aligned} \tag{3}$$

, where the fourier coefficients are de-

fined as follows:

$$a_{n,\mathbf{r}} = \frac{2}{N_i} \sum_{m=1}^{N_i} cos[n\phi_{m,\mathbf{r}}] I[r, \phi_{m,\mathbf{r}}]$$
$$b_{n,\mathbf{r}} = \frac{2}{N_i} \sum_{m=1}^{N_i} sin[n\phi_{m,\mathbf{r}}] I[r, \phi_{m,\mathbf{r}}] \quad (4)$$

The result is an image, in which every pixel is acquired during the same stimulus phase ψ. In other words, all the pixels in the reconstructed image are acquired simultaneously.

In equation (3), α is a free parameter of crucial importance. It defines how many harmonics of the primary frequency are used in the reconstruction. Therefore, α depends on the spectrum of each pixel's intensity as function of the stimulus phase. Fast changes will require a larger α than slow occuring intensity changes. Note, that the sampling theorem sets a theoretical limit to size of α, (5).

$$\alpha < \frac{N_i}{2} \quad (5)$$

Matching α to the expected intensity changes can be used to reject noise. On the other hand, underestimating α might be detrimental.

We use the presented method to investigate the sound-evoked vibration patterns of organ of Corti structures, e.g. hair cells. Therefore, we reconstruct images at equally distant consecutive phases. The quantification of the vibrations is done by an optical flow computation between two consecutive images. The algorithm basically solves the equation (6) under the assumption that the local fluorescence intensity only changes due to motion.

$$\frac{dI[\mathbf{r}, \psi]}{d\psi} = \frac{dI[\mathbf{r}, \psi]}{d\mathbf{r}} \quad (6)$$

Equation (6) presents an ill-posed problem. One way to solve it is to filter the image through different wavelet scales and build a system of equations by repeating equation (6) for all filtered images [23]. Doing so for consecutive images yields two dimensional motion estimates for every point in the image. In a final step, the trajectories are spatially and temporally convoluted with a small Gaussian kernel. This produces localized averages of the trajectories and therefore reduces noise at the cost of spatial and temporal smoothing.

2.3 INTERFEROMETRY

Interferometry is a well established technique to measure optical path differences, today mainly employed in material science. It relies on the detection of interference, which is a property of all waves, e.g. surface or electromagnetic waves. The existence of interference is a direct result of the superposition principle, meaning that the resulting wave is simply the sum of its components. In the case of light interference, the light sources need to have a fixed phase relation in order to have any observable effect. This is commonly achieved by using one source and splitting the light into different parts. After recombining the different beams again, interference occurs.

2.3.1 HOMODYNE INTERFEROMETRY

Homodyne interferometry measures the interference pattern of typically two light beams of the same frequency. Figure 2.3 illustrates the setup. The initial light beam from the source, e.g. a laser, is split into one reference and one object beam. The reference beam travels to a fixed reference mirror and is reflected back towards the beam splitter, while the object mirror reflects part of the object beam back to the beam splitter. The observed intensity of the recombined beams is directly dependent on the difference in the optical path length of the reference and object beam (Figure 2.3). Constructive interference occures when reference and object beam are in phase, giving a maximum signal at the detector (black position in Figure 2.3). Destructive interference leads to a minimal signal at the detector and occurs when the two beams are 180°out of phase (gray position in Figure 2.3). Thus, the observed intensity changes can be related to changes in the sample position, which occurs perpendicular to the object beam. A detailed mathematical description can be found in Appendix A. Note that the observed intensity is a temporal average of the actual interference pattern, since present detectors cannot resolve the frequency of light. The lower resolution limit of the homodyne interferometer is dictated by intensity noise of the light source and the shot and amplifier noise of the detector.

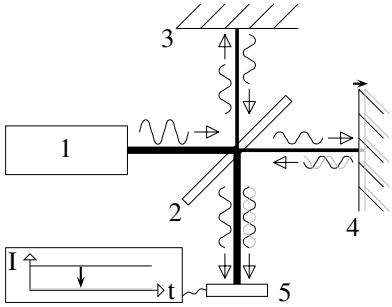

Figure 2.3: *Schematic of a typical homodyne interferometer for vibration measurements. It consists of a light source (1), beam splitter (2), reference mirror (3), probe mirror (4) and detector (5). The waveforms depict the electrical field of the light and the arrow indicates the propagation direction. As the probe mirror changes its position (from black to gray) the optical path difference changes accordingly and the observed intensity (I) decreases.*

2.3.2 HETERODYNE INTERFEROMETRY

Heterodyne interferometry is the technique of choice for high resolution non-contact vibration measurements. The setup is similar to a homodyne interferometer with one exception: the frequency of the reference beam is slightly different from the object beam. Either a fast moving sample will shift the light frequency of the object beam due to the doppler effect, or the frequency is artificially altered. The latter one has two distinct advantages for cochlear mechanics measurements. It is more sensitive to slow motion and instead of velocities it measures positions, eliminating the accumulating error from the integration of inaccurate velocities. Typically, acousto-optical modulators are used to shift the frequency of the reference beam several KHz up to tens of MHz ($\triangle$f), which is a tiny fraction of the average frequency of light ($\sim$500 THz). The recombined object and reference beam have a linear growing phase relation resulting in an interference signal, which alternates between destructive and constructive interference, a beating signal. The observed intensity ($I[t]$) at the detector is a sinusoidal function of the time with a frequency equal to the frequency shift of the reference beam:

$$I[t] := c_1 * \cos[(2\pi \triangle f)t + \theta] + c_2 \quad (7)$$

, where θ describes the phase shift due to the optical path difference between the object and reference beam. Moving the

sample adds to the phase difference between the two beams, resulting in phase modulation of the beating signal (Figure 2.4; Appendix B). In contrast to the homodyne interferometer, the information about the sample motion is now encoded in the temporal domain. The information of the sample movement is recovered by demodulation of the beating signal. We employ digital demodulation, which avoids analog electronics adding to the noise of the signal. One of the easier and more robust demodulation algorithms is the *arctan* method, which is used in Paper **II** and described in detail in Appendix B [36].

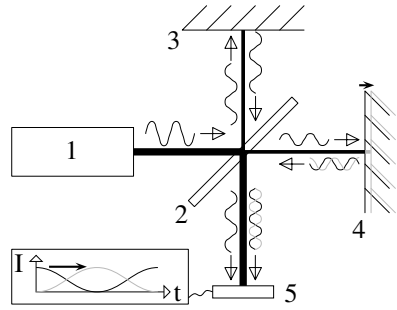

Figure 2.4: *Schematic of a typical heterodyne interferometer for vibration measurements. The frequency of the light is change by an AOM, not shown, between the beam splitter (2) and reference mirror (3). Other components are similar to Figure 2.3. Note that the observed intensity (I) is not constant over time. The phase of the signal changes accordingly to the position change of the probe mirror (from black to gray).*

3 RESULTS

The first two papers of the thesis present methodological developments, which were necessary to probe cochlear mechanics in detail. The two presented methods complement each other and are developed around a standardized measurement platform, which allows us to relate the results of the two. Paper **III** presents a multi-modal extension of both setups, combining electrical and acoustical stimulation. The paper shows spatially distinct OHC-mediated feedback on the sound-evoked vibrations of the RL. Paper **IV** uses the methodology developed in paper **III** to show that somatic electromotility is greatly influenced by the cholesterol in the OHC membrane.

3.1 RESULTS OF PAPER I

Laser scanning microscopy is too slow to be readily used to image the oscillating organ of Corti during sound stimulation. This paper presents time-resolved confocal microscopy (TRCM) method, which is an evolution of the previously published approach to reconstruct still images from an image series containing motion artifacts [24]. The calibration of TRCM shows a drastically reduced error in the subsequent optical flow calculations. In general, motion amplitudes are slightly overestimated; the overestimation increases linearly with decreasing motion amplitude. The standard deviation of the estimated motion amplitudes, which represents the measurement uncertainty, is small but increases when the motion amplitude undercuts the pixel size. Anyway, motion amplitudes as small as 10 nm can be estimated with a reasonable uncertainty. The estimation of the motion direction is very robust and yields only small errors for motion amplitudes smaller than the pixel size.

The paper also shows the relation between the motion estimation error and the number of images in the acquired image series. A larger image series means a denser sampling of the intensity signal in the phase domain, reducing the influence of intensity noise. Therefore, a decreased signal to noise ratio in the images can be at least partially compensated by increasing the number of images in the acquisition. The calibration shows that the motion estimation er-

ror quickly saturates with an increasing number of images and is essentially constant for more than eight images. The regular experiments in the cochlear apex have a slightly worse signal to noise ratio and require 12 images. The analysis of the relative small motion in the paper is based on 2 harmonics, for larger motion amplitudes higher harmonics might be beneficial.

3.2 RESULTS OF PAPER II

Paper **II** presents a heterodyne interferometer, adapted to cochlear mechanics research. The design is inspired by Cooper, but contains several novel features [11]. The presented interferometer does not depend on highly reflective targets placed on the structure of interest, but uses the small reflectivity, occuring on biological interfaces, e.g. membranes. This allows us to study cochlear mechanics without compromising cochlear physiology. The calibration of the system, using a piezoelectric transducer with strain-gauge sensor, clearly shows the interferometer's ability to resolve motion steps of sub-nm amplitude. During calibration, the intensity of the reflected beam is attenuated to mimic the situation in the inner ear. The calibration of oscillatory motion of various frequencies and amplitudes demonstrates the wide dynamic range of the system. It accurately measures motion amplitudes from sub-nm to several μm at low to moderate acoustic frequencies, 5-4000 Hz, using only a minimum number of averages. The calibration is limited to 4 KHz by the piezoelectric transducer, which shows a rapid decline of motion amplitudes for higher frequencies. One key novelty of the setup is the use of a reference interference signal, which improves the measured noise floor, especially at low frequencies (<20 Hz). The digital demodulation reduces the noise floor even further to $\leq 15\text{pm}/\sqrt{\text{Hz}}$. Furthermore, digital demodulation makes the system very versatile and easy to adapt to new tasks.

A LSM is integrated into the interferometer to allow precise localization of the interferometer measurement spot in the three dimensional structure of the organ of Corti. Additionally, the LSM is used to image the organ of Corti to

monitor morphological parameters and environment-sensitive fluorescent dyes, e.g. calcium sensing dyes. Besides the calibration, the paper provides a proof of principle experiment by validating the known relation between the motion pattern of IHC, OHC and Hensen's cells.

3.3 RESULTS OF PAPER III

Paper **III** investigates how the endogenous endocochlear potential effects cochlear mechanics. In this study we are modifying scala media polarization by injecting quasi-static currents through a glass microelectrode into scala media. Upon restoration of the positive endocochlear potential, which is lost after sacrificing the animal, the outer part of the RL (OHC3 and Hensen's cells) moves several hundred nm towards scala vestibuli. This is somewhat surprising, since a positive polarization of scala media depolarizes the OHC soma, leading to a contraction of the soma. Consequently, we expected that the RL would move towards the BM during positive current injection. Using the voltage sensitive dye RH-795 we verified that the OHCs depolarize during positive current injection. Negative polarization of scala media leads to position shifts in the opposite direct but with much smaller amplitudes as one would expect. The position shift has a fast onset and is maintained during the entire duration of the electrical stimulus (50 or 100 ms). We could not reliably estimate the proposed slow part of the position shift. The inner part of RL, OHC row one and two, moves into the opposite direction from the outer part leading to a static deformation of the RL.

Polarization of scala media simultaneously with acoustic stimulation leads to a phenomenon, which resembles cochlear amplification. During positive polarization, the sound-evoked vibrations increase, while they decrease during negative polarization. Again, there is a difference between the inner part of the organ of Corti and the outer part. Hensen's cells and row three OHCs increase the sound-evoked vibrations during positive polarization, while OHC row one shows the tendency to decrease the vibration amplitudes. We show that all the reported phenomenon require somatic electromotility, which does not ex-

clude possible contributions from the active hair bundle. Also, blocking the mechanotransduction channel in the hair bundle greatly reduces the observed position shift and abolishes any alterations of the sound-evoked vibrations during scala media polarization.

3.4 RESULTS OF PAPER IV

Paper **IV** investigates the relation between cholesterol in the OHC membrane and somatic electromotility in the intact organ of Corti. We therefore perfuse the temporal bone with methyl-β-cyclodextrin (MβCD), a water soluble compound, which has a high binding affinity for cholesterol. The cholesterol-MβCD complex has a moderate water solubility, leading to a reduction of membrane cholesterol. Control experiments showed that MβCD does not affect the passive cochlear mechanics as evidenced by stable vibration patterns and cochlear microphonics throughout drug perfusion. Cholesterol staining with filipin does not reveal any significant changes of the MβCD treated preparations, supporting the claim that there are no fundamental changes throughout the entire hearing organ.

However, MβCD perfusion greatly affects the observed position shift. Perfusion with MβCD leads to an increase in the position shift during scala media polarization. Furthermore, the relation between position shift amplitudes and applied current changes, becoming even more asymmetrical. Surprisingly, the increase in position shift amplitudes does not automatically translate into an increase in "cochlear amplification". Blocking somatic electromotility with sodium salicylate abolishes the observed effect.

4 DISCUSSION

Early on it has been recognized that electrical currents, injected into scala media, can be used to manipulate the endocochlear potential [12, 34, 46]. It has been well established that the injection of quasi-static currents (square wave) leads to scala media polarization changes without phase alterations [33]. Therefore, the temporal pattern of the polarization change roughly resembles the current injection waveform, making it possible to relate current injections with changes in scala media polarization. Noteworthy is the low-pass filtering of polarization change due to the combined electrode – scala media capacitance.

Paper **III** shows that the electrical polarization of scala media leads to a tilting of the RL with a pivot between the second and third row of OHCs. During positive polarization, the outer part of the RL (Hensen's cells and OHC row three) rapidly moves towards scala vestibuli, while it moves in the opposite direction during negative polarization. The motion amplitude is non-linear and highly asymmetric, leading to larger responses to positive scala media polarization. The asymmetry resembles the one of somatic electromotility observed in isolated outer hair cells [59]. However, the polarity of the static position shift presented in Paper III contradicts the expectations and literature [6, 2, 59]. One would expect that during positive polarization of scala media the RL moves towards scala tympani, since the conductance of the MET channels at rest leads to a depolarization of the OHC soma, which has been show to shorten isolated OHCs. Unfortunately, the used one-photon microscope could not resolve the motion of the OHC base. Hence, no definite conclusions about cell length changes can be drawn. It must be assumed that the integrated OHCs react similar to the isolated OHCs and that a complex structural refinement inside the organ of Corti is responsible for the odd polarity of the RL motion [38].

The polarity of the position shift is in accordance with the data presented by Mammano *et al*, which is the only other paper, presenting sustained position shifts of the RL in the cochlear apex

[45]. They also show that the Claudius cells, on top of the BM, move in the opposite direction during scala media polarization. This illustrates that scala media polarization leads to a structural deformation of the organ of Corti rather than a repositioning.

Electrically-evoked BM position shifts in the cochlear base indicate a pivot around the outer pillar foot [53]. The inner part of the BM (*zona arcuata*) moves in the opposite direction from the outer part (*zona pectinata*). Having a cathode in SV and an anode in ST, a configuration comparable to negative polarization of scala media, moves the *zona arcuata* towards scala media and the *zona pectinata* towards scala tympani. Similar results for the *zona pectinata* in the base were presented by Mountain *et al* [69]. However, these two studies oppose the position shift polarity of the *zona pectinata* in the cochlear apex (as observed by Mammano *et al*), making it very difficult to extrapolate BM motion for the cochlear apex from the spatially resolved BM measurements in the cochlear base during sustained electrical stimulation [45]. The contradictory measurements between cochlear apex and base could also hint to fundamental differences between the two extrema of the organ of Corti.

It is generally believed that the positive endogenous EP drives OHC electromotility, which in turn increases the organ of Corti motion. Numerous reports present evidence of positive feedback on the sound-evoked BM motion in the cochlear base, mediated by OHC electromotility (review [57]). Unfortunately, reports are rare that present evidence for feedback on the physiological relevant RL side of the organ of Corti. It is often assumed that increased BM motion amplitudes pose an increased input for the cochlear signal transduction. This assumption is based on data from the cochlear base comparing BM and auditory nerve fibre tuning [48] (but see also [19]). However, the proposed force, with which the OHCs increase the BM motion, will also act on the RL and the effect on both structures will depend on the resistance of each. Chan *et al* shows that the ratio of TM to BM motion is approximately 10 in the apex, when the

organ of Corti is electrically stimulated with a sinusoid [8]. These data illustrate that the electromotility-mediated feedback is much larger for the RL side of the apical organ of Corti. Similar findings were presented for the static position shift [45].

Again, the question arises if there are radial differences of the electromotility-mediated feedback on the sound-evoked RL vibrations. Considering our position shift data, one could envision that there are fundamental differences along the RL. Paper **III** shows a clear difference in the feedback between the OHC rows. During positive polarization of scala media, the amplitude of the sound-evoked motion increases for the outer part of the RL (OHC row two, three and Hensen's cells) and decreases during negative polarization. This polarity of the feedback is not surprising if one considers the polarity of the observed position shift. Consequently, the inner part of the RL shows the opposite feedback polarity during scala media polarization. This kind of response will increase the already existing differences in sound-evoked motion amplitudes observed along the radial direction of the RL. In the passive cochlear apex, the sound-evoked motion amplitudes of the RL are largest at the Hensen's cells and decline towards the IHCs and the difference can exceed 10 dB [40]. The increased radial differences likely increase the shearing between the RL and TM, enhancing the stimulation of the IHC bundle.
The different feedback polarity between the inner and outer part of the RL is also in agreement with Nowotny *et al* [51]. They show that the RL at OHC row two moves 180° out phase from the IHCs, with a pivot point close to the pillar head, when stimulated electrically with a sinusoid. They also show that this phenomenon is not present at the level of the TM, which explains the absence of the phase shift in [8].

The observed polarity of the OHC feedback on the RL in our measurements is supported by *in vivo* measurements in the cochlear apex [41]. In this study, the effect of the OHC feedback is derived from the comparison of RL and BM vibration data before and after the sacrifice of the animal. It is generally as-

sumed that the major factor contributing to the loss of cochlear sensitivity shortly after death is anoxia. In a few minutes, anoxia leads to a negative polarization of scala media [52]. Khanna *et al* report that after the sacrifice of the animal the motion amplitudes of the outer RL (Hensen's cells) declined, which is consistent with our data. However, they also report motion amplitudes of the BM (*zona pectinata*), which increase after the death of the animal, which opposes most measurements made in the cochlear base. This could be interpreted as major differences between the function of the active cochlea in the base and the apex (review [57]).

Pharmacological experiments validate that somatic electromotility is required for the static position shift and the dynamic alteration of the sound-evoked vibrations observed in paper **III** and **IV**. Blocking somatic electromotility or MET channels abolishes the effect of the current injections into scala media. It must be explicitly stated that the pharmacological results do not rule out any contribution from hair bundle motility. Deactivating somatic electromotility influences the hair bundle by repositioning the RL and therefore changing the reference point for hair bundle motility. Furthermore, the active hair bundle might generate the enhance receptor potential, on which somatic electromotilty acts. Hence, no definite conclusions can be drawn from the sodium salicylate experiments about the role of hair bundle motility in the presented experiments.

In paper *IV* the effect of OHC membrane cholesterol on somatic electromotility is investigated. It has been shown that the somatic electromotility associated charge movement increases and is shifted towards more depolarized membrane potentials when membrane cholesterol is reduced in isolated OHCs [55, 61]. This is not surprising as the function of many transmembrane proteins depends on the content of the surrounding membrane, e.g. specific lipids. Reduction of the OHC membrane cholesterol greatly enhanced the sustained position shift in response to scala media polarization. Furthermore, cholesterol enhances the asymmetry of the response. Interestingly, cholesterol reduction leads only in some prepara-

tions to an increased feedback of OHC electromotility on the sound-evoked vibrations of the RL. The low correlation between alterations of the position shift and RL feedback changes can be interpreted in favor of hair bundle motility.

ACKNOWLEDGEMENTS

The presented work was performed at the Center for Hearing and Communication Research, formerly in the Department of Clinical Neuroscience. I would like express wholehearted gratitude to all the people I have been working and mingling with during my time in the Center. Especially I would like to thank the following persons:

My supervisor Anders Fridberger for his generous support. He gave me the seldom found freedom to explore new ideas without looking at the immediate productivity. He also knew when to push for certain things, which I was not thrilled to do, but were necessary. I learned how to write papers and that one actually needs to repeat the experiments, even if it is not as exciting as the first one. Your advice and support are highly valued.

Mats Ulfendahl for his support and his time. Eventhough he his very busy, he had always time and helpful comments if needed.

Anna Magnusson for her help, inspiration and for bringing a fresh atmosphere to the Center. Your efforts are greatly appreciated.

Anette Fransson for being more german than swedish. It's great to have you here.

Paula Mannström for taking care of all the lab supplies. Your effort is greatly appreciated.

All the others, who helped with science, made the day at work more joyous or barely bearable. You are not forgotten, but a victim of the page charges. THANK YOU!

Letztendlich danke ich meiner Familie. Ihr wart immer da wenn ich Euch brauchte, ohne Euch wäre das nie möglich gewesen und ich werde es nie vergessen

This work was supported by the Wallenberg Foundations, the Swedish Research Council, Tysta Skolan Foundation, Hörselskadas Riksförbund and the funds of Karolinska Institutet.

REFERENCES

[1] Alberts B (1994) Molecular biology of the cell, 3th edn. Garland Publishing, New York

[2] Ashmore J.F. 1987. A fast motile response in guinea-pig outer hair cells: the cellular basis of the cochlear amplifier. J. Physiol. 388:323-47.

[3] Ashmore J.F. 2008. Cochlear outer hair cell motility. Physiol. Rev. 88:173-210.

[4] Barral J., K. Dierkes, B. Lindner, F. Jülicher, and P. Martin. 2010. Coupling a sensory hair-cell bundle to cyber clones enhances nonlinear amplification. Proc. Natl. Acad. Sci. U. S. A. 107:8079-84.

[5] von Békésy G (1960) Experiments in Hearing. New York: McGraw-Hill

[6] Brownell W.E., C.R. Bader, D. Bertrand, and Y. de Ribaupierre. 1985. Evoked mechanical responses of isolated cochlear outer hair cells. Science. 227:194-6.

[7] Brundin L., Å. Flock, S.M. Khanna, and M. Ulfendahl. 1992. The tuned displacement response of the hearing organ is generated by the outer hair cells. Neuroscience. 49:607-16.

[8] Chan D.K., and A.J. Hudspeth. 2005. Mechanical responses of the organ of corti to acoustic and electrical stimulation in vitro. Biophys. J. 89:4382-95.

[9] Corwin J.T., and M.E. Warchol. 1991. Auditory hair cells: structure, function, development, and regeneration. Annu. Rev. Neurosci. 14:301-33.

[10] Crawford A.C., and R. Fettiplace. 1985. The mechanical properties of ciliary bundles of turtle cochlear hair cells. J. Physiol. 364:359-79.

[11] Cooper N.P. 1999. An improved heterodyne laser interferometer for use in studies of cochlear mechanics. J. Neurosci. Methods 88:93-102.

[12] Dallos P., Z.G. Schoeny, D.W. Worthington, and M.A. Cheatham. 1969. Cochlear distortion: effect of direct-current polarization. Science. 164:449-51.

[13] Dallos P., N. Popper, F. Fay. 1996. Springer Handbook of Auditory Research: The Cochlea. Springer

[14] Dallos P., X. Wu, M.A. Cheatham, et al. 2008. Prestin-based outer hair cell motility is necessary for mammalian cochlear amplification. Neuron. 58:333-9.

[15] Daudet N., and M.-C. Lebart. 2002. Transient expression of the t-isoform of plastins/fimbrin in the stereocilia of developing auditory hair cells. Cell Motil. Cytoskeleton. 53:326-36.

[16] Davis H. 1965. A model for transducer action in the cochlea. Cold Spring Harbor Symp. Quant. Biol. 30:181-90.

[17] Delmas P., J. Hao, and L. Rodat-Despoix. 2011. Molecular mechanisms of mechanotransduction in mammalian sensory neurons. Nat. Rev. Neurosci. 12.

[18] Eatock R.A., D.P. Corey, and A.J. Hudspeth. 1987. Adaptation of mechanoelectrical transduction in hair cells of the bullfrog s sacculus. J. Neurosci. 7:2821-36.

[19] Evans E.F., and J.P. Wilson. 1975. Cochlear tuning properties: concurrent basilar membrane and single nerve fiber measurements. Science. 190:1218-21.

[20] Flock Å. 1965. Transducing mechanisms in the lateral line canal organ receptors. Cold Spring Harbor Symp. Quant. Biol. 30:133-45.

[21] Flock Å., and H.C. Cheung. 1977. Actin filaments in sensory hairs of inner ear receptor cells. J. Cell Biol. 75:339-43.

[22] Frank G., W. Hemmert, and A.W. Gummer. 1999. Limiting dynamics of high-frequency electromechanical transduction of outer hair cells. Proc. Natl. Acad. Sci. U. S. A. 96:4420-5.

[23] Fridberger A., J. Widengren, and J. Boutet de Monvel. 2004. Measuring hearing organ vibration patterns with confocal microscopy and optical flow. Biophys. J. 86:535-43.

[24] Fridberger A., I. Tomo, M. Ulfendahl, and J. Boutet de Monvel. 2006. Imaging hair cell transduction at the speed of sound: dynamic behavior of mammalian stereocilia. Proc. Natl. Acad. Sci. U. S. A. 103:1918-23.

[25] Fridberger A., M. Von Tiedemann, Å. Flock, B. Flock, L.-G. Ofverstedt, and U. Skoglund. 2009. Three-dimensional structure of outer hair cell pillars. Acta Oto-Laryngol. 129:940-5.

[26] Gafni M., and H. Sohmer. 1976. Intermediate endocochlear potential levels induced by hypoxia. Acta Oto-Laryngol. 82:354-8.

[27] Gillespie P.G., and U. Müller. 2009. Mechanotransduction by hair cells: models, molecules, and mechanisms. Cell. 139:33-44.

[28] Gold T (1948) Hearing. II. The Physical Basis of the Action of the Cochlea. Proc. R. Soc. Lond. B. Biol. Sci. 135(8): 492-498.

[29] Hagiwara S. 1963. Electron Microscope Study on the Vestibular Membrane (Reissner). Arch. Histol. Jpn. Nippon soshikigaku kiroku. 24:187-227.

[30] Harris G.G., L.S. Frishkopf, and Å. Flock. 1970. Receptor potentials from hair cells of the lateral line. Science. 167:76-9.

[31] Hibino H., F. Nin, C. Tsuzuki, and Y. Kurachi. 2010. How is the highly positive endocochlear potential formed? The specific architecture of the stria vascularis and the roles of the ion-transport apparatus. Pfluegers Arch. 459:521-33.

[32] Holley M.C., and J.F. Ashmore. 1988. A cytoskeletal spring in cochlear outer hair cells. Nature. 335:635-7.

[33] Honrubia V., and P.H. Ward. 1970. Mechanism of production of cochlear microphonics. J. Acoust. Soc. Am. 47:498-503.

[34] Hubbard A.E., and D.C. Mountain. 1983. Alternating current delivered into the scala media alters sound pressure at the eardrum. Science. 222:510-2.

[35] Jacob S., I. Tomo, A. Fridberger, J. Boutet De Monvel, and M. Ulfendahl. 2007. Rapid confocal imaging for measuring sound-induced motion of the hearing organ in the apical region. J. Biomed. Opt. 12:021005.

[36] Jacob S., C. Johansson, M. Ulfendahl, and A. Fridberger. 2009. A digital heterodyne laser interferometer for studying cochlear mechanics. J. Neurosci. Methods 179:271-7.

[37] Jaeger R.G., J. Fex, and B. Kachar. 1994. Structural basis for mechanical transduction in the frog vestibular sensory apparatus: II. The role of microtubules in the organization of the cuticular plate. Hear. Res. 77:207-15.

[38] Karavitaki K.D., and D.C. Mountain. 2007. Imaging electrically evoked micromechanical motion within the organ of corti of the excised gerbil cochlea. Biophys. J. 92:3294-316.

[39] Kazmierczak P., H. Sakaguchi, J. Tokita, E.M. Wilson-Kubalek, R. a Milligan, U. Müller, and B. Kachar. 2007. Cadherin 23 and protocadherin 15 interact to form tip-link filaments in sensory hair cells. Nature. 449:87-91.

[40] Khanna S.H., Å. Flock, and M. Ulfendahl. 1989. Changes in cellular tuning along the radial axis of the cochlea. Acta Oto-Laryngol., Suppl. 457:163-73

[41] Khanna S.M., and L.F. Hao. 2000. Amplification in the apical turn of the cochlea with negative feedback. Hear. Res. 149:55-76.

[42] Khimich D., R. Nouvian, R. Pujol, S. Tom Dieck, A. Egner, E.D. Gundelfinger, and T. Moser. 2005. Hair cell synaptic ribbons are essential for synchronous auditory signalling. Nature. 434:889-94.

[43] Korade Z., and A.K. Kenworthy. 2008. Lipid rafts, cholesterol, and the brain. Neuropharmacology. 55:1265–1273.

[44] Liberman M.C., J. Gao, D.Z.Z. He, X. Wu, S. Jia, and J. Zuo. 2002. Prestin is required for electromotility of the outer hair cell and for the cochlear amplifier. Nature. 419:300-4.

[45] Mammano F., and J.F. Ashmore. 1993. Reverse transduction measured in the isolated cochlea by laser Michelson interferometry. Nature. 365:838-41.

[46] Mountain D.C. 1980. Changes in endolymphatic potential and crossed olivocochlear bundle stimulation alter cochlear mechanics. Science. 210:71-2.

[47] Nadol J.B. 1988. Comparative anatomy of the cochlea and auditory nerve in mammals. Hear. Res. 34:253-66.

[48] Narayan S.S., A.N. Temchin, A. Recio, and M.A. Ruggero. 1998. Frequency tuning of basilar membrane and auditory nerve fibers in the same cochleae. Science. 282:1882-4.

[49] Nguyen T.V., and W.E. Brownell. 1998. Contribution of membrane cholesterol to outer hair cell lateral wall stiffness. Otolaryngol. Head. Neck. Surg. 119:14–20

[50] Nin F., H. Hibino, K. Doi, T. Suzuki, Y. Hisa, and Y. Kurachi. 2008. The endocochlear potential depends on two K+ diffusion potentials and an electrical barrier in the stria vascularis of the inner ear. Proc. Natl. Acad. Sci. U. S. A. 105:1751-6.

[51] Nowotny M., and A.W. Gummer. 2006. Nanomechanics of the subtectorial space caused by electromechanics of cochlear outer hair cells. Proc. Natl. Acad. Sci. U. S. A. 103:2120-5.

[52] Nuttall A.L., and M. Lawrence. 1980. Endocochlear potential and scala media oxygen tension during partial anoxia. Am. J. Otolaryngol. 1:147-53.

[53] Nuttall A.L., M. Guo, and T. Ren. 1999. The radial pattern of basilar membrane motion evoked by electric stimulation of the cochlea. Hear. Res. 131:39-46.

[54] Pickles J.O., S.D. Comis, and M.P. Osborne. 1984. Cross-links between stereocilia in the guinea pig organ of Corti, and their possible relation to sensory transduction. Hear. Res. 15:103-12.

[55] Rajagopalan L., J.N. Greeson, A. Xia, et al. 2007. Tuning of the outer hair cell motor by membrane cholesterol. J. Biol. Chem. 282:36659-70.

[56] Ricci A.J., B. Kachar, J.E. Gale, and S.M. Van Netten. 2006. Mechano-electrical transduction: new insights into old ideas. J. Membr. Biol. 209:71-88.

[57] Robles L., and M.A. Ruggero. 2001. Mechanics of the mammalian cochlea. Physiol. Rev. 81:1305-52.

[58] Rzadzinska A.K., M.E. Schneider, C. Davies, G.P. Riordan, and B. Kachar. 2004. An actin molecular treadmill and myosins maintain stereocilia functional architecture and self-renewal. J. Cell Biol. 164:887-97.

[59] Santos-Sacchi J. 1989. Asymmetry in voltage-dependent movements of isolated outer hair cells from the organ of Corti. J. Neurosci. 9:2954-62.

[60] Sewell W.F. 1984. The relation between the endocochlear potential and spontaneous activity in auditory nerve fibres of the cat. J. Physiol. 347:685-96.

[61] Sfondouris J., L. Rajagopalan, F.A. Pereira, and W.E. Brownell. 2008. Membrane composition modulates prestin-associated charge movement. J. Biol. Chem. 283:22473-81.

[62] Smith C.A., O.H. Lowry, and M.L. Wu. 1954. The electrolytes of the labyrinthine fluids. The Laryngoscope. 64:141-53.

[63] Smith C.A., and F.S. Sjöstrand. 1961. A synaptic structure in the hair cells of the guinea pig cochlea. J. Ultrastruct. Res. 5:184–192.

[64] Steel K.P. 1983. The tectorial membrane of mammals. Hear. Res. 9:327-59.

[65] Tilney M.S., L.G. Tilney, R.E. Stephens, C. Merte, D. Drenckhahn, D. a Cotanche, and a Bretscher. 1989. Preliminary biochemical characterization of the stereocilia and cuticular plate of hair cells of the chick cochlea. J. Cell Biol. 109:1711-23.

[66] Tilney L.G., M.S. Tilney, and D.J. DeRosier. 1992. Actin filaments, stereocilia, and hair cells: how cells count and measure. Annu. Rev. Cell Biol. 8:257-74.

[67] Wang X., S. Yang, S. Jia, and D.Z.Z. He. 2010. Prestin forms oligomer with four mechanically independent subunits. Brain Res. 1333:28-35.

[68] Wever E.G., J.G. McCormick, J. Palin, and S.H. Ridgway. 1971. The cochlea of the dolphin, Tursiops truncatus: hair cells and ganglion cells. Proc. Natl. Acad. Sci. U. S. A. 68:2908-12.

[69] Xue S., D.C. Mountain, and A.E. Hubbard. 1995. Electrically evoked basilar membrane motion. J. Acoust. Soc. Am. 97:3030-41.

[70] Yu N., M.L. Zhu, and H.B. Zhao. 2006. Prestin is expressed on the whole outer hair cell basolateral surface. Brain Res. 1095:51-8.

[71] Zheng J., W. Shen, D.Z.Z. He, K.B. Long, L.D. Madison, and P. Dallos. 2000. Prestin is the motor protein of cochlear outer hair cells. Nature. 405:149-55.

[72] Zheng L., G. Sekerková, K. Vranich, L.G. Tilney, E. Mugnaini, and J.R. Bartles. 2000. The deaf jerker mouse has a mutation in the gene encoding the espin actin-bundling proteins of hair cell stereocilia and lacks espins. Cell. 102:377-85.

[73] Zine A., A. Hafidi, and R. Romand. 1995. Fimbrin expression in the developing rat cochlea. Hear. Res. 87:165-9.

A HOMODYNE INTERFEROMETRY

Assuming that the electric field (Ψ) of the incident light can be described as a sinusoidal function and the coherence length of the source is infinite. Then the electric field of the incident light can be given by:

$$\Psi[t] = 2A\sin[\omega t + (\frac{2\pi}{\lambda})x], \tag{8}$$

where x is the optical length, t the time , $2A$ the amplitude, λ the wavelength and ω the frequency of the incident light. Assuming no losses at the beam splitter and the mirrors, the recombined beam (Φ) can be described as a sum of the object (o) and the reference beam (o):

$$\begin{aligned}\Phi[t] &= o[t] + o[t] \\ &= A\sin[\omega t + \phi_1] + A\sin[\omega t + \phi_2],\end{aligned} \tag{9}$$

with phase offsets

$$\phi_{1/2} = \frac{2\pi d_{1/2}}{\lambda}, \tag{10}$$

where $d_{1/2}$ denotes the optical path length of the object and reference beam, respectively. The intensity (I) at the detector can then be calculated by:

$$I[t] = \langle\Phi^2\rangle_T = A^2(1 + cos[\frac{2\pi}{\lambda}(d_1 - d_2)]), \tag{11}$$

where $\langle.\rangle_T$ denotes the average of time, reflecting the fact that the detector is typically too slow to resolve the high frequency of the light oscillation.

B HETERODYNE INTERFEROMETRY

Let I denote the intensity at the detector.

$$I[t] = \langle (o + r)^2 \rangle_T [t] \tag{12}$$

where $\langle . \rangle_T$ defines a time integration over a time T, which is the exposure time of the detectors. T is inversely proportional to the highest resolvable frequency of the detector.
The object beam reaching the detector is defined as o, and r denotes the reference beam.

$$\begin{aligned} o[t] &= O_1 \cos[\omega_o t + \varphi_o[t]] \\ r[t] &= R_1 \cos[\omega_r t + \varphi_r] \end{aligned} \tag{13}$$

ω_o and ω_r is the frequency of the light in the object and reference beam, respectively, $\phi_o[t]$ and ϕ_r are the phase offsets in the object and reference beam at the detector. The phase offset of the object beam is a function of time due to the moving sample and therefore changes in the optical path of the object beam.
By inserting equation (13) in (12), a relation for the intensity at the detector is obtained:

$$\begin{aligned} I[t] &= \frac{1}{2}(O^2 + R^2) + 2mOR\langle \cos[\omega_r t + \varphi_r] \cos[\omega_o t + \varphi_o[t]] \rangle_T \\ I[t] &= \frac{1}{2}(O^2 + R^2) + mOR\langle \cos[(\omega_o + \omega_r)t + (\varphi_o[t] + \varphi_r)] \rangle_T \\ &\quad + mOR\langle \cos[(\omega_o - \omega_r)t + (\varphi_o[t] - \varphi_r)] \rangle_T \end{aligned} \tag{14}$$

m denotes the mixing parameter, which characterizes how much of the object and reference beam interfere. Since the order of ω_o and ω_r is THz while $\frac{1}{T}$ is of order

MHz, the second summand in equation (14) can be neglected.

$$\langle \cos[(\omega_o + \omega_r)t + (\varphi_o[t] + \varphi_r)] \rangle_T \simeq 0 \tag{15}$$

The difference of ω_o and ω_r can range between KHz and a few MHz, and is determined by the frequency shifting of the reference beam:

$$2\pi \triangle f \equiv |\omega_o - \omega_r| \tag{16}$$

The detector should be at least fast enough to clearly resolve this frequency. Using equation (15) and (16), (14) can be transformed to:

$$I[t] = \frac{1}{2}(O^2 + R^2) + mOR\cos[(2\pi \triangle f)t + (\varphi_o[t] - \varphi_r)]. \tag{17}$$

Thus, we can define the general phase offset θ as

$$\theta := \varphi_o[t] - \varphi_r. \tag{18}$$

By filtering the ac component from the signal, one can further simplify (17).

$$I[t] := c * \cos[(2\pi \triangle f)t + \theta[t]] \tag{19}$$

In equation (19), the measured intensity is related to the optical path difference between the reference and object beam. By defining a constant phase offset θ_0 as follows:

$$\theta_0 = \theta[0], \tag{20}$$

the time varying phase offset due to the sample motion can be uncoupled from the optical path difference between the reference and object beam. θ_0 results mainly from the different length of the interferometer's object and reference arm.

Therefore, equation (19) can be rewritten:

$$I[t] := c * \cos[(2\pi \triangle f)t + \theta_0 + \theta'[t]], \tag{21}$$

with:

$$\theta'[t] = \theta[t] - \theta_0 \tag{22}$$

The displacement (s) is related to the phase offset θ' by:

$$s[t] = \frac{\lambda \theta'[t]}{4\pi n}, \tag{23}$$

where n denotes here the refractive index of the immersion fluid.

The demodulation is based on the so called *arctan* method. This method involves digital signal processing and can be performed on a standard computer in reasonable time.
The measured interference signal ($I[t]$) can be described as a sinusoidal function of time

$$I[t] := c * \cos[(2\pi \triangle f)t + \theta[t]] \tag{24}$$

and was derived in the previous section. Let $s[t]$ be the analysis in-phase signal and $c[t]$ the analysis quadrature signal defined as follows:

$$\begin{aligned} s[t] &:= A \sin[(2\pi \triangle f)t + \varphi_0] \\ c[t] &:= A \cos[(2\pi \triangle f)t + \varphi_0] \end{aligned} \tag{25}$$

Multiplying equation (24) with (25) yields the equations stated in (26).

$$\begin{aligned} s[t]I[t] &= cA \sin[(2\pi \triangle f)t + \varphi_0] \cos[(2\pi \triangle f)t + \theta[t]] \\ c[t]I[t] &= cA \cos[(2\pi \triangle f)t + \varphi_0] \cos[(2\pi \triangle f)t + \theta[t]] \end{aligned} \tag{26}$$

Applying trigonometric product-sum identities leads again to a separation of high and low frequency terms:

$$\begin{aligned} s[t]I[t] &= \frac{1}{2}cA(\sin[(4\pi\triangle f)t + \varphi_0 + \theta[t]] + \sin[\varphi_0 - \theta[t]]) \\ c[t]I[t] &= \frac{1}{2}cA(\cos[(4\pi\triangle f)t + \varphi_0 + \theta[t]] + \cos[\varphi_0 - \theta[t]]) \end{aligned} \tag{27}$$

To remove the high frequency sinusoidal waves one can simply use a low pass filter with a cut off frequency much higher than the highest vibration frequency of the sample one is interested in, but much lower than the carrier frequency $\triangle f$. We then obtain:

$$\begin{aligned} s[t]I[t] &\overset{lowpass}{\longrightarrow} s^*[t] := \frac{1}{2}cA\sin[\varphi_0 - \theta[t]] \\ c[t]I[t] &\overset{lowpass}{\longrightarrow} c^*[t] := \frac{1}{2}cA\cos[\varphi_0 - \theta[t]] \end{aligned} \tag{28}$$

Dividing these two signals and taking the arctan leads to:

$$\arctan\frac{s^*[t]}{c^*[t]} = \varphi_0 - \theta[t] \tag{29}$$

By setting φ_0 to $\theta[0]$, one can adjust the analysis signals to the interference signal. Applying equation (23) yields the measured displacement of the sample.

$$s[t] = \frac{\lambda}{4\pi n}\arctan\frac{s^*[t]}{c^*[t]}, \tag{30}$$